PAPER • OPEN ACCESS

Nuclear data libraries for IFMIF-DONES neutronic calculations

To cite this article: E. Mendoza *et al* 2022 *Nucl. Fusion* **62** 106026

View the article online for updates and enhancements.

Nuclear data libraries for IFMIF-DONES neutronic calculations

E. Mendoza[1,*] ⓘ, D. Cano-Ott[1] ⓘ, A. Ibarra[1,2] ⓘ, F. Mota[1] ⓘ, I. Podadera[1,2] ⓘ,
Y. Qiu[3] and S.P. Simakov[3]

[1] Centro de Investigaciones Energéticas Medioambientales y Tecnológicas (CIEMAT), Madrid, Spain
[2] Consorcio IFMIF-DONES España, Granada, Spain
[3] Karlsruhe Institute of Technology (KIT), Karlsruhe, Germany

E-mail: emilio.mendoza@ciemat.es

Abstract

International Fusion Materials Irradiation Facility-DEMO Oriented NEutron Source
(IFMIF-DONES) is an installation aimed to irradiate with a high neutron flux materials
relevant for the construction of the DEMOnstration fusion power plant (DEMO), in order to
study the damage due to irradiation. Neutrons are generated using a 40 MeV and 125 mA
deuteron beam impinging on a thick liquid lithium target. With these characteristics, damage
due to irradiation comparable to that in the first wall of a fusion power reactor is achieved. In
this paper we investigate the differences in the neutronic calculations of the IFMIF-DONES
design when using different nuclear data libraries. We first studied the differences in neutron
production due to Li(d, xn) reactions between different models and evaluations, comparing the
different results with experimental data. Additionally, we tested the performance of the
MCNP6.2 and Geant4 Monte Carlo codes when using deuteron incident data libraries. Then,
we performed neutronic calculations of the IFMIF-DONES design using the most
reliable Li(d, xn) neutron production models available, which are the FZK-2005 and
JENDL/DEU-2020 evaluations according to the results obtained in the first part of the study.
Thus, the differences in these evaluations are propagated to different neutronic calculation
results: neutron flux, primary displacement damage, gas production, and heating in the
materials to be irradiated. Finally, we also carried out these same neutronic calculations while
using different nuclear data libraries for the neutron transport.

Keywords: IFMIF-DONES, neutronics, D-Li neutron source, D-Li data library, MCNP6.2,
Geant4, fusion

(Some figures may appear in colour only in the online journal)

1. Introduction

Future fusion power plants will generate neutron fluxes in the
order of 10^{14} cm^{-2} s^{-1}, with a peak energy of 14.1 MeV, and,
at present, there is no facility worldwide capable of generatng
a similar flux. However, it is necessary to perform radiation

damage studies in nuclear fusion materials for the design and
licensing of future fusion reactors. This is the main purpose of
the International Fusion Material Irradiation Facility-DEMO
Oriented NEutron Source (IFMIF-DONES) [1], a facility that
is in the design and prototyping phase and whose objective
is to produce a neutron flux with an intensity and an energy
spectrum suitable for irradiating materials for the design of
fusion reactors, and in particular, for the DEMOnstration
fusion Power Plant (DEMO) [2].

Neutrons are produced in IFMIF-DONES by bombarding
a liquid lithium target with a 40 MeV deuteron beam, which

is provided by an accelerator with a nominal CW deuteron current of 125 mA. A test cell confines the target chamber and test modules, located with a minimum gap in the neutrons forward direction, where the neutron flux is very intense ($\sim$1–5 $\times$ 10^{14} cm^{-2} s^{-1}).

Neutronic calculations are obviously one of the key pieces of the IFMIF-DONES design. They are needed to optimize the neutron source, obtain the activation of the different components for safety assessments and maintenance strategies, shielding calculations, waste management, etc. To date, these calculations have mainly been done with the MCNP code [3] or with some of its extensions, such as MCUNED [4] and McDeLicious [5], all of them relying on data libraries to model the deuteron and neutron induced reactions. Specifically, the FZK-2005 evaluation [6, 7] has been used to model the Li(*d*, *xn*) reactions, and the FENDL data library [8] has been used for the transport of the generated neutrons, especially version FENDL-3.1d [9].

In this work, we investigated the differences in the neutronic calculations, which are obtained using alternative data libraries. Since Li(*d*, *xn*) reactions are the key to modeling the neutron source, in section 2 we review the data libraries and models available for the Li(*d*, *xn*) reactions, and compare their performance with the available experimental data. Next, in section 3, we take the best Li(*d*, *xn*) neutron production models to perform neutronic calculations of IFMIF-DONES, and we study the differences in the obtained neutron fluxes, primary displacement damage, gas production, and heating in the test cell. Afterward, in section 4, we focus on the impact it has on the results using one or another neutron library. To do this, we make calculations similar to those in the previous section, but in this case changing between different data libraries for the neutron transport. Finally, we summarize the main conclusions of this study in section 5.

2. Modeling of Li(*d*, *xn*) reactions

2.1. Experimental data and evaluations

There are two experimental datasets concerning neutron production by 40 MeV deuterons impinging on a thick Li target in the EXFOR database [10]:

(a) The data provided by Hagiwara *et al* (2005) [11]. They irradiated a thick (21.4 mm) ^{nat}Li sample with 40 MeV deuterons and provide both the neutron yields and energy spectra at nine different angles between 0° and 110° [12].

(b) The data provided by Saltmarsh *et al* (1977) [13]. They irradiated a thick ^{nat}Li sample with 40 MeV deuterons and provide total neutron yields, integrated above 2 MeV neutron energy, at seven different angles between 0° and 90°.

An additional dataset has been reported by Fischer *et al* in [7, 14] from Mann *et al* (1981) [15] (40 MeV deuterons on a thick Li target), but it is not in EXFOR and not publicly available. According to [7], the neutron yield reported by Mann *et al* at forward angles is slightly smaller than the values from Hagiwara *et al* (referred to as Baba *et al* in [7]), and

both the yields and the energy spectra are very similar in both experiments at 30° and 60°.

Concerning the evaluations of the Li(*d*, *xn*) reactions, at the moment there are basically two. One has been performed by researchers of the Karlsruhe Institute of Technology (KIT) [6, 7], and is referred to as the FZK-2005 evaluation in this paper. This is the one used by the McDeLicious code [5], which is currently the standard tool used in neutronic calculations of the IFMIF-DONES facility design to model the deuteron-lithium neutron source [16–20]. McDeLicious is an extension of MCNP with the ability of generating source neutrons based on d + Li interactions. The second one is the JENDL/DEU-2020 evaluation [21, 22], which has been released recently.

In addition to these two evaluations, there is an additional one in ENDF/B-VII.1 [23], but this evaluation goes just up to 5 MeV incident deuteron energy for ^{6}Li and up to 20 MeV for ^{7}Li, i.e. it does not cover the energy range under study. This evaluation is also adopted by TENDL-2019 [24].

In other releases of the TENDL library, the deuteron incident ^{6,7}Li data files come from calculations preformed with the TALYS code [25] only, without taking into account any experimental data. This is the case of TENDL-2011 [26], which has been adopted by FENDL-3.1d [8, 9]. In this case, the data in the library goes up to 200 MeV. However, according to the TALYS/TENDL developers [27], the nuclear data files in TENDL-2011 are not expected to be very reliable for light nuclei ($A < 20$). The latest release of FENDL at the time of writing this paper, FENDL-3.2 [28], adopts the JENDL/DEU-2020 data library for incident deuterons.

2.2. Transport codes

We simulated with the MCNP6.2 [3] and Geant4 [29, 30] Monte Carlo transport codes the experiment performed by Hagiwara *et al*, using both the FZK-2005 and JENDL/DEU-2020 evaluations. This serves both to compare the evaluations with the experimental results and to check the performance of the Monte Carlo codes when using these data libraries.

In order to run MCNP6.2 with these evaluations, it is necessary to have the data files, originally distributed in ENDF-6 format [31], in ACE format, which is the one used by MCNP6.2. For JENDL/DEU-2020 we took the ACE files provided by the authors in [32]. For FZK-2005 we tried to perform the conversion with the standard versions of NJOY21 and NJOY2016 [33], but we found some errors during the processing of the files. Due to this, we had to make some modifications to the NJOY source code. Once these issues were sorted out, it was finally possible to perform the conversion to the ACE format. These modifications were reported to the NJOY developers to be included in future releases. In the case of Geant4, the conversion of the ENDF-6 format files to the G4NDL format, the one used by Geant4, was performed with a tool developed by the authors for previous works [34].

The neutron energy spectra at the nine different angles provided by Hagiwara *et al* are compared with the results of the MCNP6.2 simulations in figure 1. The figure shows that both libraries reproduce the experimental results very reasonably, although there are some differences. To show them better, the
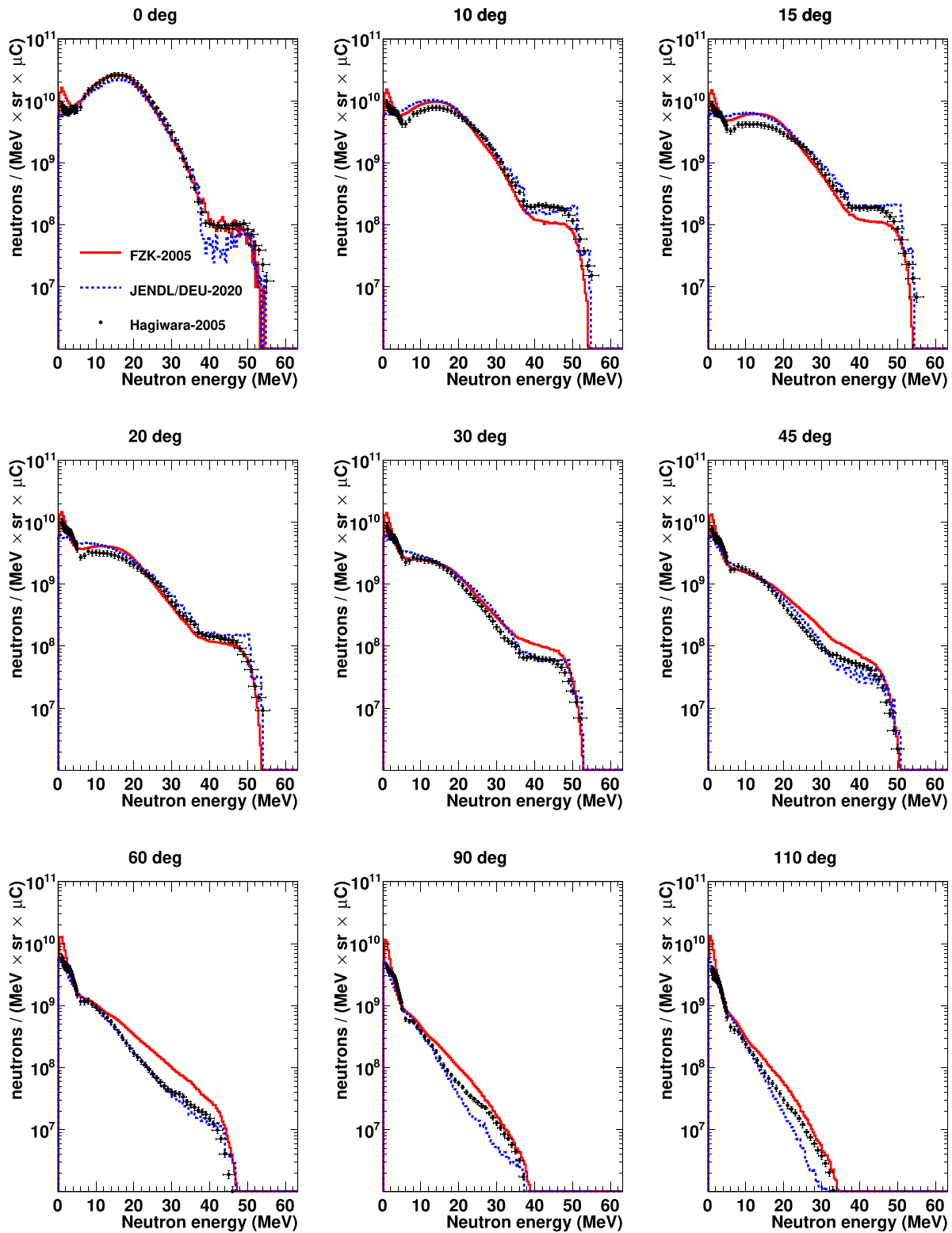
Figure 1. Energy spectra of the neutrons emitted at different angles due to Li(*d, xn*) reactions in the irradiation of a thick Li sample using 40 MeV deuterons. The experimental results reported by Hagiwara *et al* are presented together with the results from MCNP6.2 using the FZK-2005 and JENDL/DEU-2020 data libraries.

same graphs but with the *Y*-axis on a linear scale are presented in figure 2, for the three smallest angles. The error bars in the Hagiwara *et al* experimental data correspond to total uncertainties, including both uncertainties due to counting statistics and due to systematic effects. The size of these uncertainties is 10%–15%. The neutron yields as a function of the emission angle are presented in figure 3, at small angles since they are the most relevant for IFMIF-DONES. The experimental
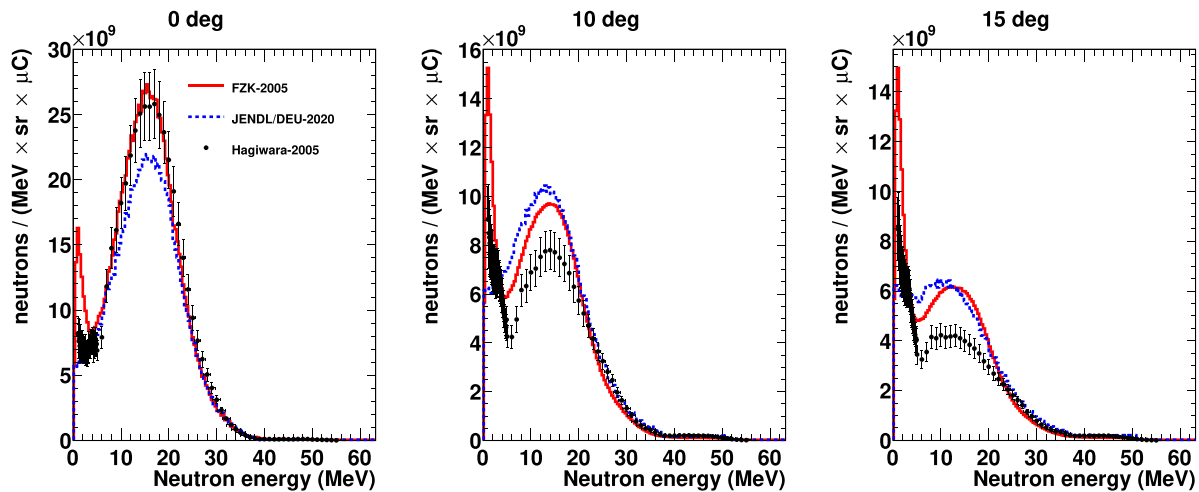
Figure 2. Same as the top panels of figure 1, but with the *Y*-axis in linear scale.
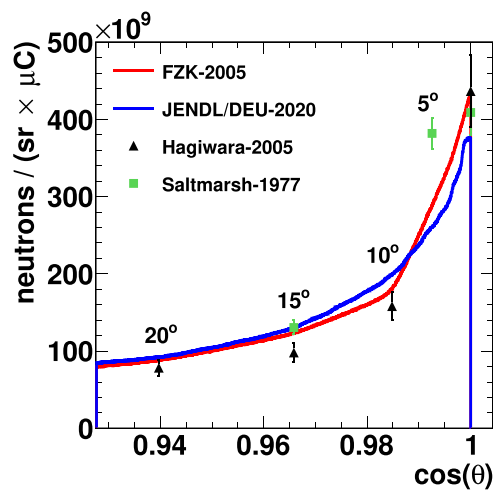

Figure 3. Neutron yields as a function of the emission angle obtained in the irradiation of a thick Li sample using 40 MeV deuterons. An energy threshold of 2 MeV has been considered, which is the one present in the Saltmarsh *et al* data.

results from Saltmarsh *et al* have also been included in this comparison.

According to these results, FZK-2005 reproduces very well the spectra from Hagiwara *et al* at small angles and above 5 MeV, but seems to overestimate the neutron production at small neutron energies and at large angles. JENDL/DEU-2020 gives apparently similar results, but without the aforementioned discrepancies in the FZK-2005 evaluation at low energies and large angles.

Although the calculations performed with both evaluations reproduce the experimental data quite well, it must be taken into account that the experimental values have uncertainties of 10%–15%, according to the authors of the Hagiwara *et al* experiment. In addition, it is not at all obvious how to interpolate between different angles, especially between 10° and 0°. If the neutron yields shown in figure 3 are integrated between 20° and 0°, we obtain 3.78×10^9 (FZK-2005), 3.79×10^9 (JENDL/DEU-2020, +0.3%), 3.50×10^9 (Hagiwara, −8%),

and 4.91×10^9 (Saltmarsh, +30%) neutrons per μC. The values in parenthesis show the differences with respect to FZK-2005, and a linear interpolation between the data points has been assumed to compute the integrals of the experimental data. If the value of Saltmarsh at 5° is added to the Hagiwara data points, then the integral becomes 3.74×10^9 neutrons per μC, i.e. it increases by 7% (−1%, when comparing to FZK-2005).

Given the uncertainties estimated by the authors of the experiments, and the differences in neutron production, depending on whether one data is used or another, it may be reasonable to estimate ∼15% of the uncertainty in the neutron production in a thick Li target due to 40 MeV deuterons when performing calculations with the FZK-2005 and JENDL/DEU-2020 evaluations. This is an estimate of the average uncertainty, since there is a dependence on energy and angle. A similar value (20%) was assessed in [7] to the neutron production obtained with McDeLicious (i.e. FZK-2005).

Concerning Geant4, we performed simulations similar to those of MCNP6.2 to reproduce the Hagiwara *et al* experiment. The results obtained with the FZK-2005 library at first were very different from those obtained with MCNP6.2, and therefore with the values of Hagiwara *et al*. After investigating the problem, we discovered a bug in the Geant4 ParticleHP package, which is the model that manages the low energy nuclear data libraries. After correcting this bug, the results obtained with Geant4 are practically the same as those obtained with MCNP6.2, as shown in figure 4. These fixes have been included in the standard Geant4 distribution as of version Geant4.10.7.p03. The results obtained with JENDL/DEU-2020 are the same as those obtained with MCNP6.2, except that oscillating structures appear in the neutron emission spectra. These structures can be seen in figure 4 and are not due to statistical fluctuations. This issue will be investigated in the future.

Figure 4 also shows the performance of different MCNP6.2 and Geant4 models when simulating the neutron production
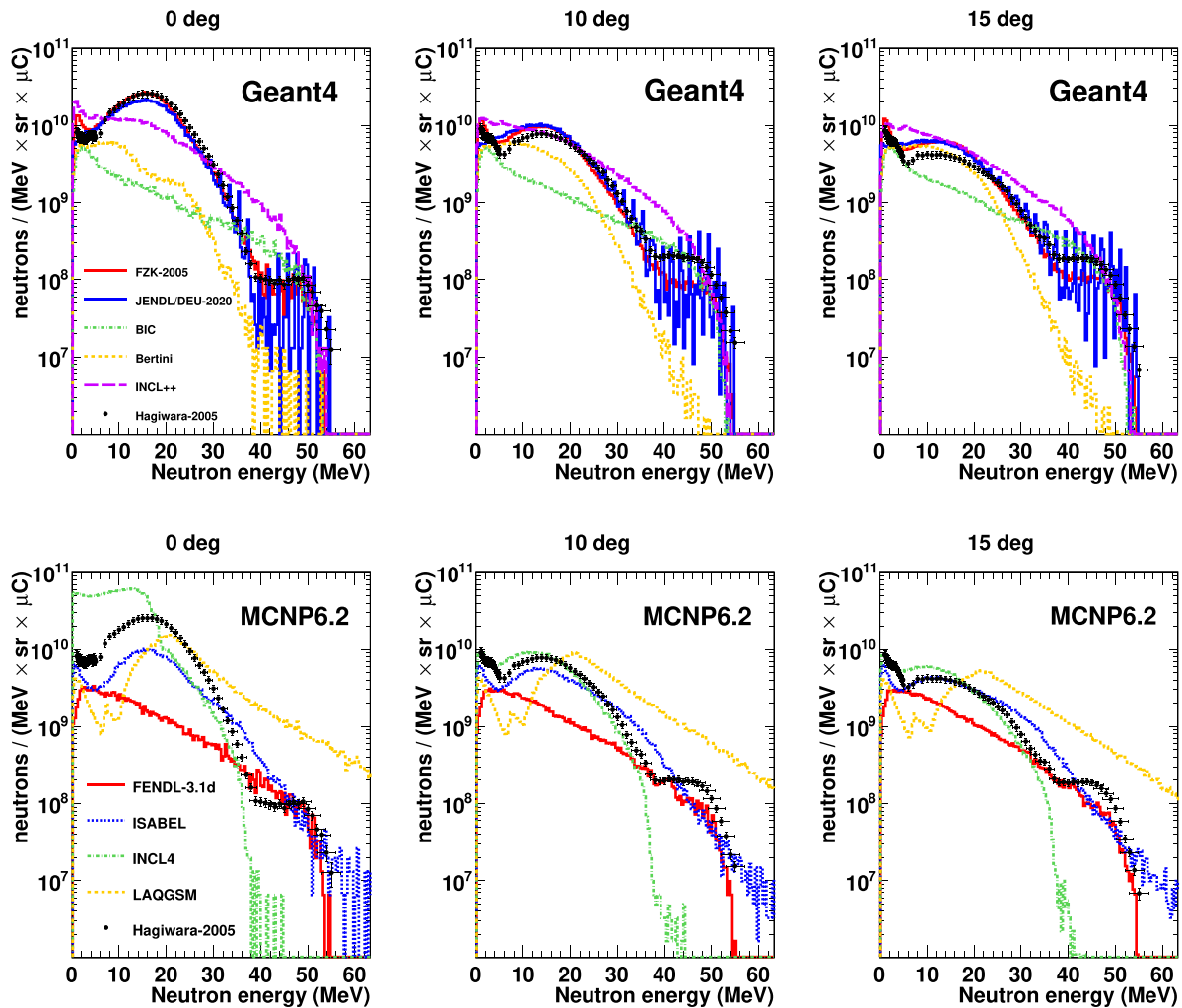
Figure 4. Same as figure 1, but using different models and data libraries in Geant4 (top) and MCNP6.2 (bottom) calculations.

due to Li(*d*, *xn*) reactions. With Geant4 (version Geant4.10.6) we tested the binary cascade (BIC), Bertini, and INCL++ models; and with MCNP6.2 the ISABEL, INCL4 and LAQGSM03.03 models. We also performed simulations with the FENDL-3.1d (i.e. TENDL-2011) data library. In all these cases, the experimental results reproduced are much worse than the results obtained when using the FZK-2005 and JENDL/DEU-2020 evaluations, and therefore it is not worth using them for simulating DONES. There is at least one model whose performance seems to be much better [35] than the models tested in this work, but at this moment it is not available in Geant4 or MCNP.

3. Neutronic calculations of IFMIF-DONES with different neutron sources

In the next part of the study we perform neutronic calculations of the IFMIF-DONES facility design using different neutron sources. The calculations were performed with MCNP6.2, using the same detailed geometry (version mdl9.2.0) as in previous works [16–20]. Figure 5 shows a horizontal cut view of the geometry at the position of the lithium target.
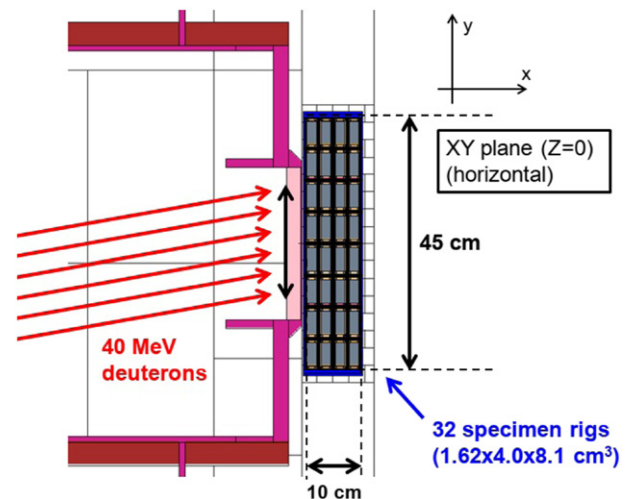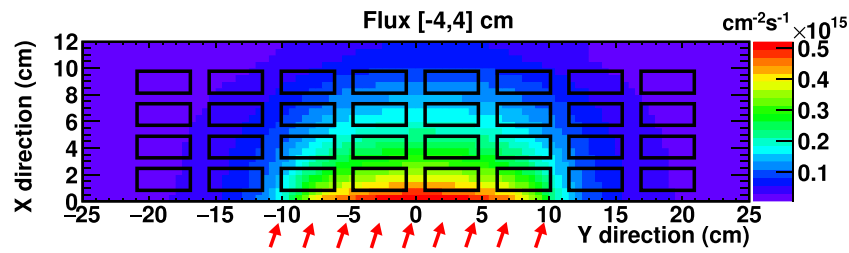

Figure 5. Horizontal cut view of the IFMIF-DONES geometry implemented in MCNP6.2 at the level of the center of the deuteron beam.

The deuteron beam, presented with red arrows, impinges into the liquid lithium target with an angle of 9°. A stack of 32 specimen rigs are located inside the so-called high flux

Figure 6. Neutron flux in the HFTM obtained from MCNP6.2 calculations, averaged in the vertical direction between −4 and +4 cm with respect to the center of the deuteron beam. The FZK-2005 library was used to model the Li(d, xn) reactions.

test module (HFTM) just after the lithium target to irradiate the materials with the highest neutron flux. We have used the reference deuteron beam profile in the IFMIF/EVEDA phase, which has a footprint on a 20×5 cm^2 area, and a nominal intensity of 125 mA.

Different quantities have been tallied in a $12 \times 50 \times 10$ cm^3 Cartesian mesh covering the HFTM with 0.5 cm resolution in each coordinate. These quantities are the neutron flux, the primary displacement damage, the H and He production, and the nuclear heating. The same quantities have also been calculated averaged in each specimen bin. The primary displacement damage rate has been obtained by multiplying the neutron flux by the DPA cross section of natural iron provided by the JEFF-3.3/DPA library [36, 37], using the arc-dpa approach, which is available in reaction channel MT = 900 [31]. The H and He production rates were obtained by multiplying the neutron flux by the total proton (MT = 203) and total alpha (MT = 207) production cross sections of Eurofer-97, the European reference material for the first wall of a DEMO fusion reactor [38], in a similar way to how it has been done in previous works [18]. The nuclear heating has been obtained from an energy deposition mesh tally (TMesh tally type 3 [3]). All the calculations presented in this section has been performed using FENDL-3.1d for the neutron transport and for computing the MT = 203 and 207 cross sections.

The simulations have been carried out using deuterons as source particles. To model the Li(d, xn) reactions, the FZK-2005 library has been used in one simulation, and JENDL/DEU-2020 in another. An example of the obtained results is presented in figure 6. There we show the neutron flux in the HFTM as a function of the position in the horizontal plane, averaged at ±4 cm in the vertical direction, which corresponds, in good approximation, to the size of the specimen rigs ($1.62 \times 4 \times 8.1$ cm^3). The red arrows in the bottom of the figure represent the deuteron beam, which impinge into the lithium target between $y = -10$ and $+10$ cm (see figure 5). The black rectangles inside the figure show the positions of the specimen rigs.

To compare the values obtained in both simulations, we show the ratio between different quantities in figure 7. Similarly to figure 6, the ratios are given as a function of the position in the horizontal plane, averaged at ±4 cm in the vertical direction. We show the ratios obtained for the total neutron flux, primary displacement damage, H and He production, heating, and He/dpa ratio. In the case of the nuclear heating, there is a part of the figure that appears in white

color. This part corresponds to a place where no material is defined in the MCNP6.2 geometry and therefore there is no energy deposition (the rest of the quantities are computed by multiplying the neutron flux by some specific cross section). The He/dpa ratio is the ratio between the He production and the primary displacement damage.

For the specimen rigs in the *center*, those located between $y = -10$ and $+10$ cm, i.e., just in front of the deuteron beam, the obtained results agree within ∼10%. The differences in the specimen rigs on the *sides*, those located below $y = -10$ cm or above $y = +10$ cm, are much larger, reaching up to 60%. This agrees with the results presented in the previous section, where it is shown that the differences between the two libraries increase with the neutron emission angle (figure 1). The specimen rigs in the sides are most sensitive to the neutrons emitted at large angles. It is worth mentioning that the rigs in the center are for material irradiation and those in the sides are intended for diagnosis or to be used as reflectors.

We also constructed an additional neutron source based on the Hagiwara *et al* dataset, hereafter referred to as the 2D-Hagiwara neutron source. In it, neutrons are generated with a uniform probability distribution along a 2 cm depth inside the lithium target (which corresponds to the range of 40 MeV deuterons), in the direction of the deuteron beam and using the same footprint as in the previous simulations, i.e. the same 2D beam profile. The energy and momentum direction of the source neutrons are obtained from a 2D-probability distribution generated from the nine neutron emission spectra provided by Hagiwara *et al* (experimental values of figure 1) and assuming a linear interpolation between them.

In the 2D-Hagiwara neutron source some approximations are made: the linear interpolation to construct the 2D-energy-angular distribution, the initial position of the neutrons are sampled uniformly, the interaction of the neutrons with the Li target is not treated properly, etc. In order to estimate the impact of these effects on the IFMIF-DONES neutronic calculations, we built two additional neutron sources. Both in exactly the same way as the 2D-Hagiwara neutron source, but using, instead of the Hagiwara *et al* data points, the spectra obtained from the MCNP6.2 simulations of the Hagiwara *et al* experiment. The first neutron source was obtained from the simulations performed with the FZK-2005 library (i.e. the red simulated spectra of figure 1), and the second neutron source from the simulations performed with the JENDL/DEU-2020 library (i.e. the blue simulated spectra of figure 1). Simulations
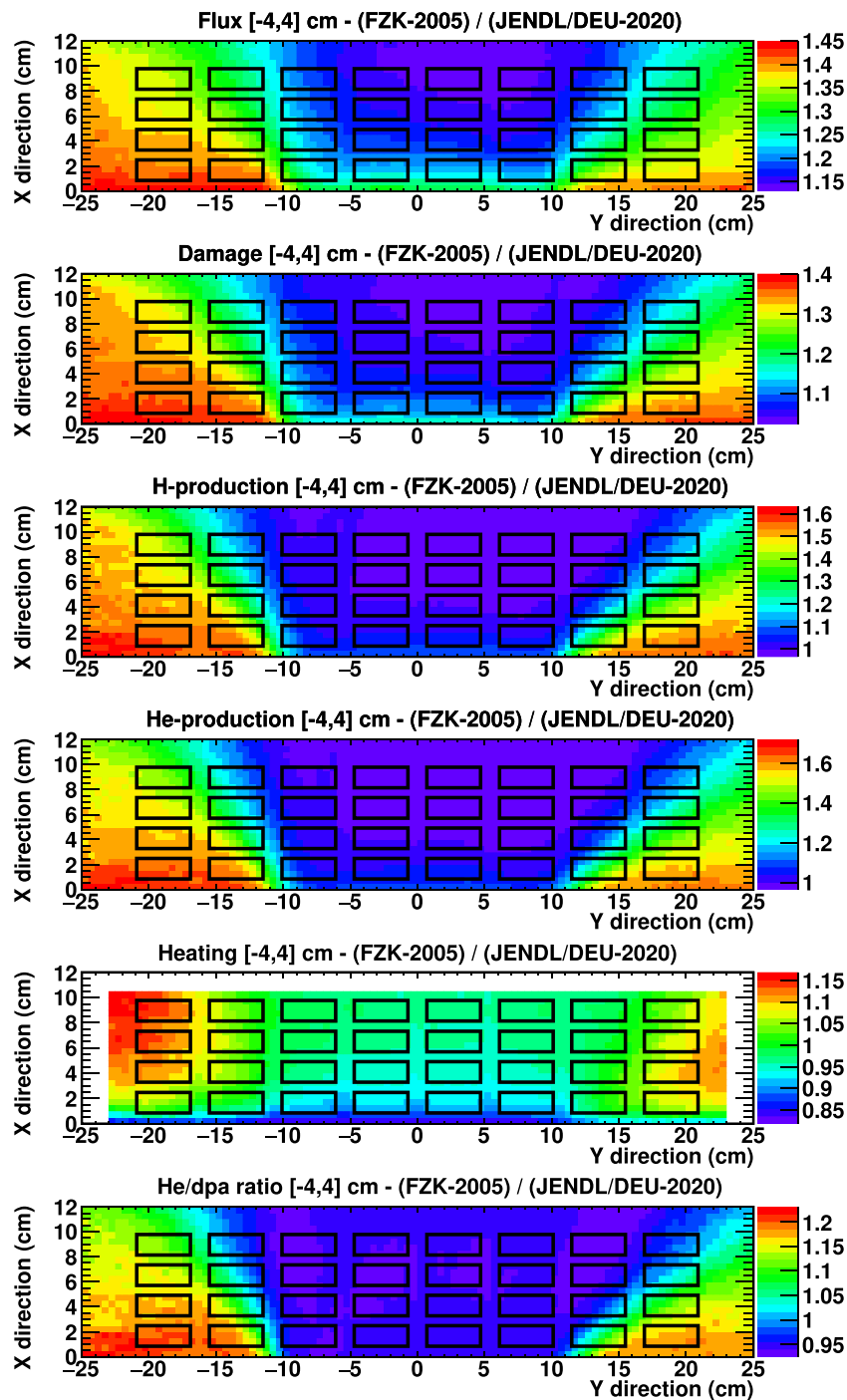
Figure 7. From top to bottom: neutron flux, primary displacement damage, H and He production, nuclear heating, and He/dpa ratio in the HFTM obtained from MCNP6.2 calculations with FZK-2005 divided by the results obtained with JENDL/DEU-2020. All the results have been averaged in the vertical direction between −4 and +4 cm with respect to the center of the deuteron beam.

of IFMIF-DONES were then performed with these two neutron sources and the results were compared with the results obtained when simulating deuterons as source particles and the same library (FZK-2005 or JENDL/DEU-2020, depending on the case) to model the Li(*d*, *xn*) reactions. These comparison showed that, when using the same data library, the results (flux, primary displacement damage, gas production, and heating) obtained using both approaches were compatible within ∼5%. Thus, we estimate at 5% the uncertainty in the results obtained

with the 2D-Hagiwara neutron source due to the mentioned effects.

When comparing the results of the simulations performed with the 2D-Hagiwara neutron source with the ones using FZK-2005 and JENDL/DEU-2020, we found that the results obtained with 2D-Hagiwara are, in general, closer to the ones obtained with JENDL/DEU-2020 than to those obtained with FZK-2005, especially in the specimen rigs on the sides. An example is provided in figure 8, where we show the same
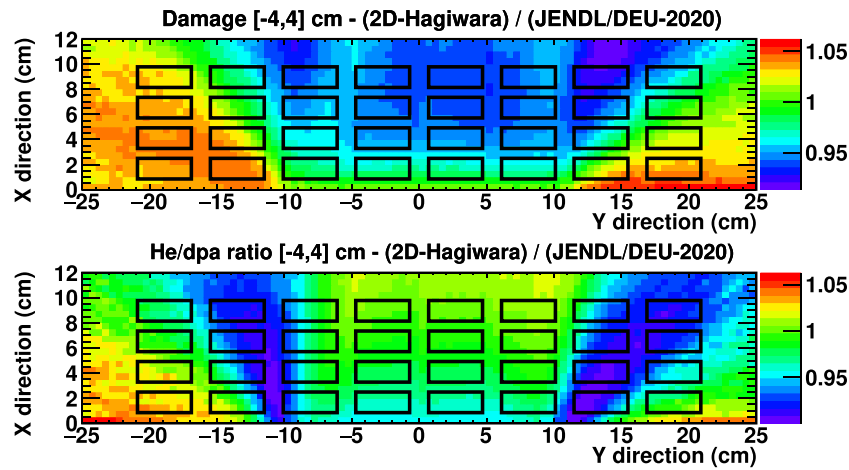
Figure 8. Primary displacement damage (top) and He/dpa ratio (bottom) in the HFTM obtained from MCNP6.2 calculations when using the 2D-Hagiwara neutron source divided by the results obtained with deuterons as source particles and JENDL/DEU-2020. All the results have been averaged in the vertical direction between −4 and +4 cm with respect to the center of the deuteron beam.
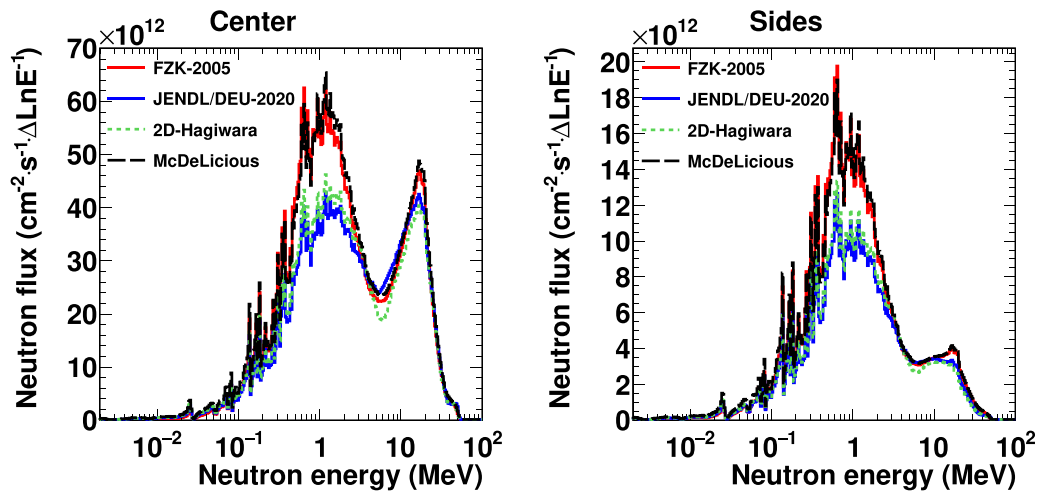
Figure 9. Neutron flux per unit lethargy (ΔLnE, which means that the bin contents have been divided by the natural logarithm of the ratio between the upper and lower bin limits) averaged in the specimen rigs in the center (left), i.e. those located between $y = -10$ and $y = +10$ cm, and in the specimen rigs in the sides (right), i.e. the rest. The results are provided for MCNP6.2 calculations using three different neutron sources and for McDeLicious.

comparison as in figure 7, but replacing FZK-2005 with 2D-Hagiwara and only for the primary displacement damage and the He/dpa ratio. The discrepancies in the specimen rigs on the sides in figure 7 are much smaller than the ones in figure 8, probably because JENDL/DEU-2020 reproduces with larger accuracy the neutron emission at large angles reported by Hagiwara *et al* than FZK-2005.

We also compared the results obtained with FZK-2005 with those obtained with the McDeLicious code, which are expected to be very similar since they are, in principle, using the same nuclear data. McDeLicious is a modification of MCNP that only affects the generation of source particles, the rest does not change and we also used FENDL-3.1d in McDeLicious for the neutron transport. We obtained that the neutron flux, primary displacement damage, and gas production provided by McDeLicious is ∼5% larger than the one provided by the standard version of MCNP6.2 when

using FZK-2005 in the central part of the HFTM ($-10 < y < 10$ cm), and ∼3% larger in the sides ($10 < y < -10$ cm). When computing the He/dpa ratio the results are compatible within 1%–2% in the full HFTM.

We show in figure 9 the neutron flux, as a function of the energy, averaged inside the specimen rigs in the central part of the HFTM and in the sides. Although the spectra obtained with the standard version of MCNP6.2 using FZK-2005 and McDeLicious are very similar in shape, the integrated flux from McDeLicious is 3%–5% larger, which explains the conclusions reported in the previous paragraph. We investigated the origin of these discrepancies and we found that the stopping power of deuterons in lithium in MCNP6.2 is ∼2% larger than in McDeLicious in the energy range of interest, which explains part of the observed discrepancies. The rest are probably coming from small differences in the nuclear reaction modeling. Figure 9 also shows that the neutron spectra
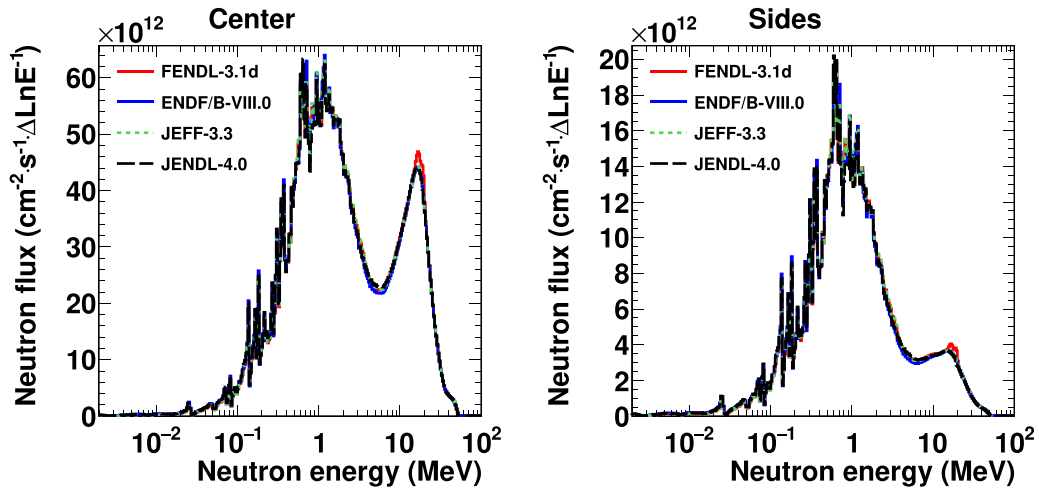
Figure 10. Same as figure 9, but using the FZK-2005 library to model the Li(*d*, *xn*) reactions and different libraries for the neutron transport.
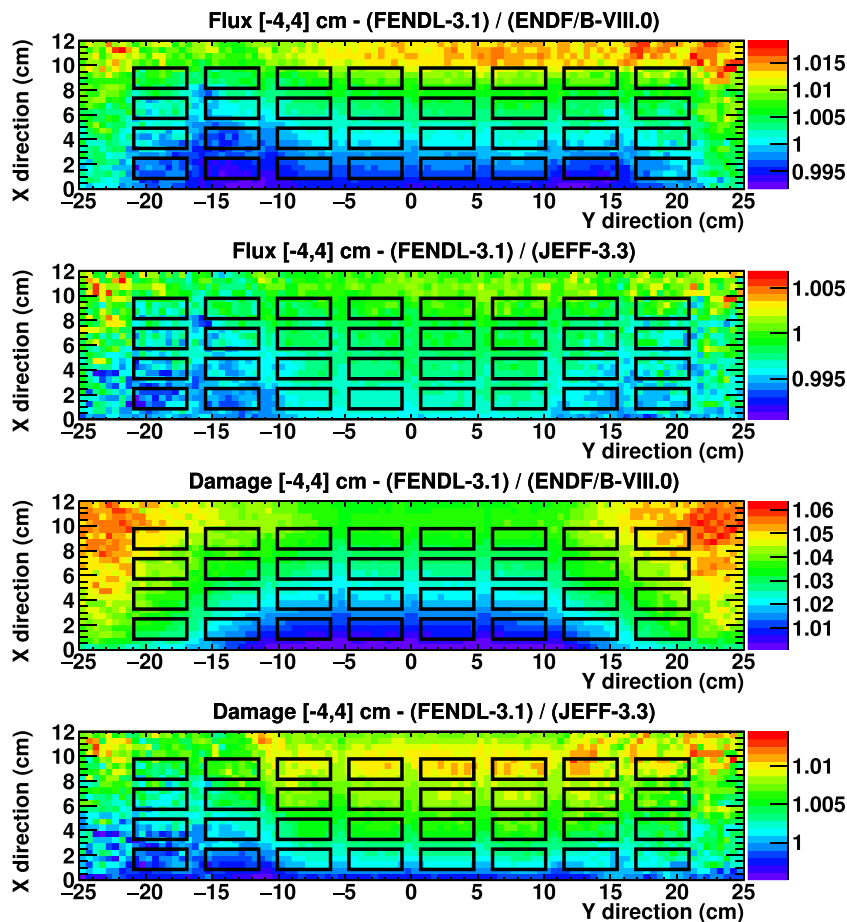
Figure 11. Neutron flux and primary displacement damage in the HFTM obtained from MCNP6.2 calculations with the FENDL-3.1d library for the neutron transport divided by the results obtained when using ENDF/B-VIII.0 or JEFF-3.3. All the results have been averaged in the vertical direction between −4 and +4 cm with respect to the center of the deuteron beam.
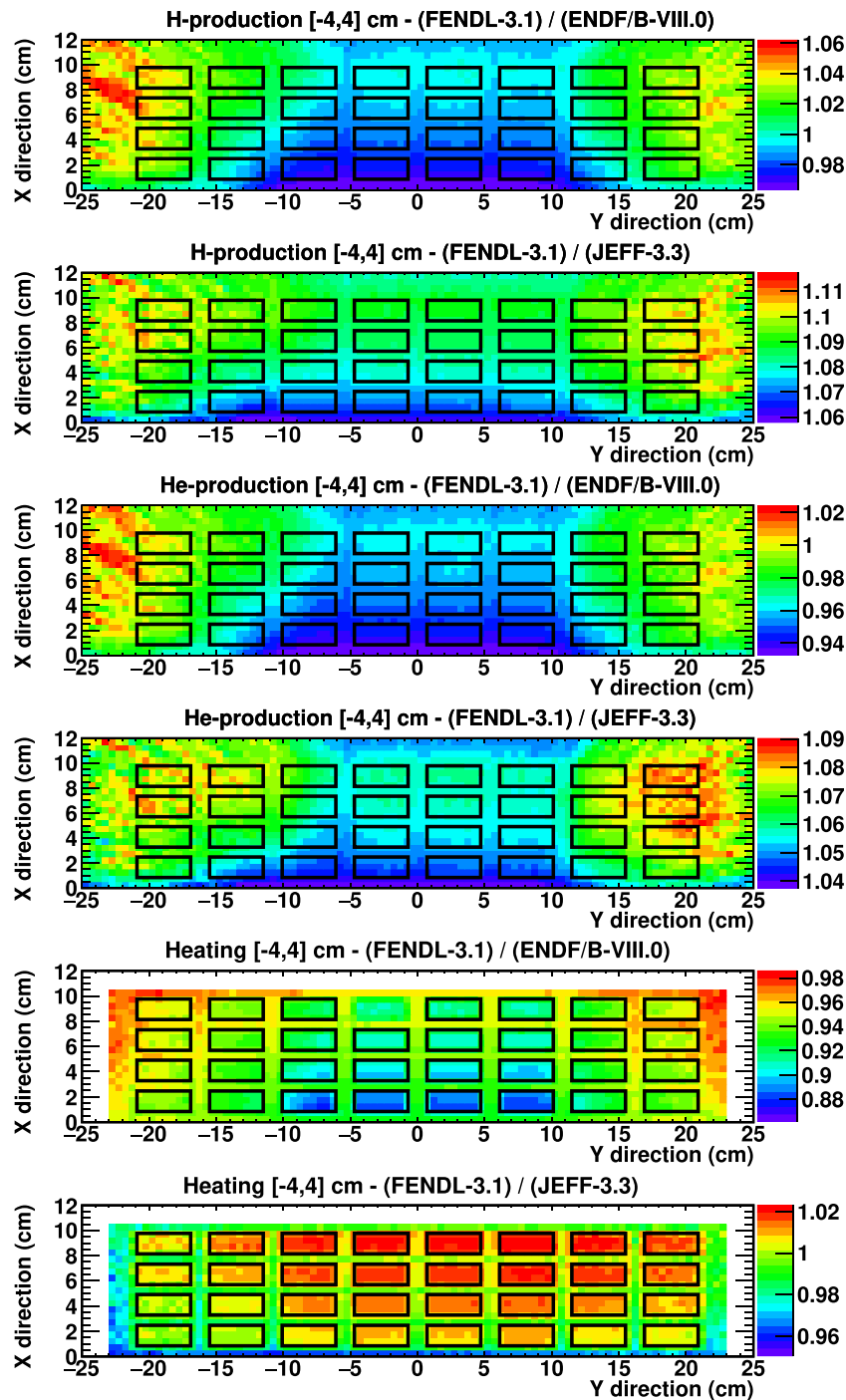
Figure 12. Same as figure 11, but for the H and He production and nuclear heating.

4. Neutronic calculations of IFMIF-DONES with different neutron transport data libraries

In the last part of the study we performed MCNP6.2 neutronic calculations of the IFMIF-DONES facility design using different libraries for the neutron transport. We made identical

from 2D-Hagiwara are closer to JENDL/DEU-2020 than FZK-2005, especially at low neutron energies, as expected from the conclusions reported in section 2.

simulations to those of the previous section, but now changing between the FENDL-3.1d, ENDF/VIII.0 [39], JEFF-3.3 and JENDL-4.0 [40] data libraries for the neutron transport. The FZK-2005 library has been used to model the Li(d, xn) reactions in all the results shown in this section. We have, however, made all these calculations with the JENDL/DEU-2020 library and the 2D-Hagiwara neutron source as well. The differences between results of calculations carried out with different transport libraries are practically the same, regardless of the neutron source used. For example, when we compare JEFF-3.3 with FENDL-3.1d, we show the calculations
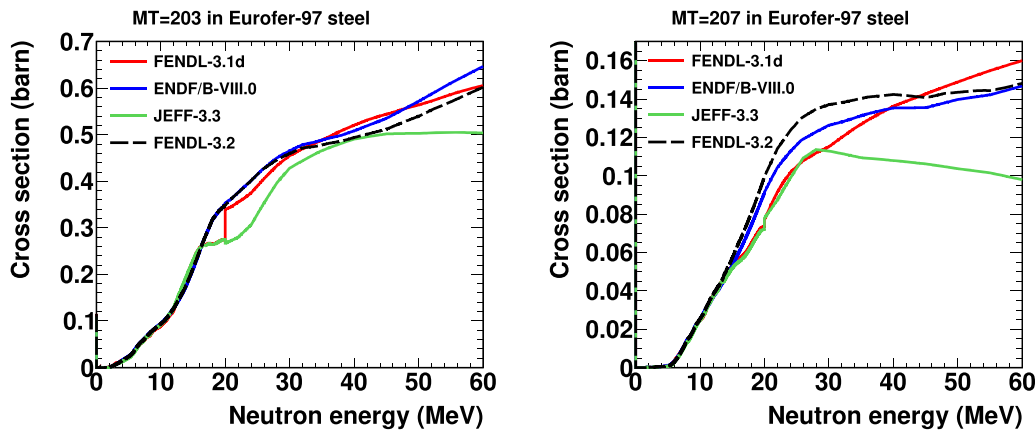
Figure 13. Total H production cross section (MT = 203, left) and total He production cross section (MT = 207, right) in Eurofer-97 provided by the FENDL-3.1d, ENDF/B-VIII.0, JEFF-3.3, and FENDL-3.2 neutron data libraries.

made with FZK-2005, but practically the same differences are observed with JENDL/DEU-2020. In the same way, the results presented in the previous section do not depend significantly on the transport library used.

Concerning the neutron transport data libraries, it should be mentioned that, with the exception of FENDL-3.1d, the energy range covered by them does not extend for every isotope to 55–60 MeV, the maximum energy of neutrons that are generated in Li(*d*, *xn*) reactions. In particular, all the isotopes in FENDL-3.1d have data up to at least 60 MeV, although in many cases there is data up to 150 or 200 MeV. The maximum energies in ENDF/VIII.0 and JEFF-3.3 also depend on the isotope, but in both cases the maximum energy can be as low as 20 MeV. The data of all JENDL-4.0 isotopes extends to 20 MeV only, making this library unsuitable for doing IFMIF-DONES neutronic calculations. To transport the neutrons out of the energy range of the libraries, MCNP6.2 uses models. In this work we used the models that are defined by default.

The obtained results show that the dependence of the resulting neutron flux in the HFTM with the neutron library is much smaller than with the deuteron library. Figure 10 shows the neutron flux averaged inside the specimen rigs, as a function of the neutron energy, obtained when using these four data libraries. The obtained spectra are more similar to each other than those in figure 9. The obtained fluxes are also compared in the two panels on the top of figure 11. There the total neutron flux obtained with ENDF/B-VIII.0 and JEFF-3.3 are compared to FENDL-3.1d, as a function of the position in the horizontal plane. The results inside the specimen rigs are compatible within 1%, which is a much larger agreement than when comparing FZK-2005 and JENDL/DEU-2020 (figure 7). A similar agreement is also obtained when using JENDL-4.0.

To understand this result, it must be taken into account that the mean free path of neutrons in lithium is between 10 and 20 cm in the energy range of interest, except for energies close to the Li resonance at 200–400 keV, where it drops down to 2 cm. The width of the lithium target is just bit more than 2 cm, so the vast majority of neutrons pass through it without interacting, reaching the HFTM with the energy with which they were generated. The mean free path of neutrons in the

HFTM, which has a width of 10 cm (figure 5), is approximately between 3 and 6 cm in the energy range of interest. The dominant reaction channels are (n, n) and (n, n′). This means that, on average, two to three interactions per neutron are expected inside the HFTM. Unless the cross sections are very different from one library to another, more collisions are usually needed to produce significant differences in the neutron flux.

Similar comparisons to those made with the flux, but with the primary displacement damage, H and He production, and nuclear heating, are presented in figures 11 and 12. Starting with the nuclear heating, the values obtained with ENDF/B-VIII.0 are ∼5%–10% larger than with FENDL-3.1d, and those of JEFF-3.3 are compatible within ∼2% with FENDL-3.1d. In the case of the primary displacement damage, the differences between ENDF/B-VIII.0 and FENDL-3.1d are up to 5%, while between JEFF-3.3 and FENDL-3.1d they do not exceed 1%. Concerning the H production, ENDF/B-VIII.0 gives values compatible with FENDL-3.1d within 2%–3%, and JEFF-3.3 gives ∼10% smaller values. For the He production, ENDF/B-VIII.0 gives values around 2%–5% larger than FENDL-3.1d, depending on the position, and JEFF-3.3 between 3% and 7% smaller. Consequently, the H and He production obtained with ENDF/B-VIII.0 are ∼10%–12% larger than with JEFF-3.3.

The differences obtained for the H and He production are significantly larger than for the primary displacement damage. This is because all three quantities are obtained by multiplying the neutron flux by a cross section. However, while for the primary displacement damage the same cross section has been used in all the cases (DPA cross section of natural iron in JEFF-3.3/DPA), a different cross section has been used to calculate the H and He production in each simulation, which is obtained from the data library used for the neutron transport. Thus, the observed differences in the H and He production are mainly due to differences in the total H and He production cross sections, and not to differences in the neutron flux.

These cross sections are presented in figure 13 for the three data libraries mentioned in this discussion and also including FENDL-3.2, which is the last release of FENDL at the time of writing this paper. The results obtained with JENDL-4.0 have been omitted as the cross sections only go up to 20 MeV. In

Table 1. H and He production rates in different elements (Ele), obtained with different neutron data libraries. The second and sixth columns (Pr) provide, respectively, the number of ^{1}H and ^{4}He particles generated per second and per material gram obtained with FENDL-3.2, assuming that the material is located in the central specimen rigs of the HFTM. The rest of the values correspond to the ^{1}H and ^{4}He production obtained, respectively, with FENDL-3.1d (R_{31d}), JEFF-3.3 (R_{J33}) and ENDF/B-VIII.0 (R_{E80}), divided by the value obtained with FENDL-3.2.

	^{1}H production				^{4}He production			
Ele	Pr (at/(s·g))	R_{31d}	R_{J33}	R_{E80}	Pr (at/(s·g))	R_{31d}	R_{J33}	R_{E80}
Li	4.9×10^{10}	1.00	—	—	2.1×10^{12}	1.00	—	—
Be	3.9×10^{10}	1.00	—	—	4.4×10^{12}	1.00	—	—
B	6.7×10^{10}	1.34	—	—	2.3×10^{12}	0.99	—	—
C	4.0×10^{10}	1.00	1.22	1.21[a]	1.8×10^{12}	1.00	0.85	1.18[a]
N	4.1×10^{11}	1.00	1.62	1.62	6.8×10^{11}	1.00	1.05	1.05
O	2.5×10^{11}	0.41	0.41	0.41	6.2×10^{11}	0.85	0.85	0.89
F	1.5×10^{11}	1.00	—	—	6.5×10^{11}	1.00	—	—
Ne	1.5×10^{11}	—	0.99	0.99	8.4×10^{11}	—	1.01	1.01
Na	3.0×10^{11}	1.00	—	—	1.8×10^{11}	1.00	—	—
Mg	3.0×10^{11}	1.00	—	—	3.3×10^{11}	1.00	—	—
Al	3.1×10^{11}	1.00	1.00	1.00	1.3×10^{11}	1.00	1.00	1.00
Si	3.8×10^{11}	1.00	—	1.00	2.0×10^{11}	1.00	—	1.00
P	5.2×10^{11}	1.00	1.00	0.57	1.4×10^{11}	1.00	0.99	0.73
S	5.7×10^{11}	1.00	1.05	—	4.4×10^{11}	1.02	1.02	—
Cl	5.6×10^{11}	1.00	—	—	1.8×10^{11}	1.00	—	—
Ar	2.9×10^{10}	1.00	—	—	2.0×10^{10}	1.00	—	—
K	5.8×10^{11}	1.00	1.00	—	2.0×10^{11}	1.00	1.00	—
Ca	6.8×10^{11}	1.00	1.06	1.12	2.2×10^{11}	1.00	0.87	0.96
Sc	2.2×10^{11}	1.00	0.89	—	3.3×10^{10}	1.00	0.95	—
Ti	9.1×10^{10}	1.00	0.97	—	2.1×10^{10}	1.00	1.26	—
V	7.2×10^{10}	1.00	0.85	—	9.4×10^{9}	1.00	1.80	—
Cr	1.0×10^{11}	1.00	1.00	1.10	5.0×10^{10}	0.55	0.55	0.54
Mn	6.3×10^{10}	1.00	1.08	1.00	1.6×10^{10}	1.00	1.21	1.00
Fe	1.4×10^{11}	0.96	0.90	1.00	3.2×10^{10}	0.90	0.88	1.00
Co	9.9×10^{10}	1.00	—	—	2.0×10^{10}	1.00	—	—
Ni	4.1×10^{11}	1.00	—	1.01	5.8×10^{10}	1.00	—	1.00
Cu	1.4×10^{11}	1.00	0.82	1.18	2.1×10^{10}	1.00	1.08	1.05
Zn	1.6×10^{11}	1.00	0.96	—	7.0×10^{10}	1.00	0.90	—
Ga	4.7×10^{10}	1.00	1.03	—	1.4×10^{10}	1.00	0.85	—
Ge	3.6×10^{10}	1.00	0.70	—	1.1×10^{10}	1.00	1.08	—
Br	3.6×10^{10}	0.98	0.98	—	5.1×10^{9}	0.95	1.08	—
Y	2.5×10^{10}	0.97	—	—	5.2×10^{9}	0.81	—	—
Zr	3.2×10^{10}	1.00	0.87	—	4.8×10^{9}	1.00	1.29	—
Nb	3.3×10^{10}	1.00	0.91	0.98	7.5×10^{9}	1.00	0.67	0.60
Mo	4.7×10^{10}	1.00	—	—	5.8×10^{9}	1.00	—	—
Rh	2.7×10^{10}	1.00	—	—	5.0×10^{9}	1.00	—	—
Ag	1.5×10^{10}	1.00	—	—	3.7×10^{9}	1.00	—	—
Cd	1.1×10^{10}	0.94	—	—	2.8×10^{9}	0.81	—	—
Sn	8.0×10^{9}	0.92	—	—	2.2×10^{9}	0.87	—	—
Sb	7.8×10^{9}	0.91	—	—	2.0×10^{9}	0.83	—	—
I	7.5×10^{9}	1.00	—	—	8.4×10^{8}	1.00	—	—
Cs	8.2×10^{9}	0.74	—	—	1.5×10^{9}	0.63	—	—
Ba	4.4×10^{9}	1.09	—	—	2.5×10^{9}	0.61	—	—
La	3.2×10^{9}	1.00	—	—	1.7×10^{9}	1.00	—	—
Ce	6.5×10^{9}	0.92	—	—	2.7×10^{9}	0.72	—	—
Sm	6.3×10^{9}	—	—	—	2.1×10^{9}	—	—	—
Gd	4.5×10^{9}	0.93	—	—	1.5×10^{9}	0.82	—	—
Er	3.3×10^{9}	0.96	—	—	1.1×10^{9}	0.61	—	—
Lu	4.7×10^{9}	0.91	1.06	—	1.4×10^{9}	0.91	0.93	—
Hf	3.6×10^{9}	0.89	—	—	1.2×10^{9}	0.65	—	—

(continued on next page)

Table 1. Continued.

Ele	Pr (at/(s·g))	R_{31d}	R_{J33}	R_{E80}	Pr (at/(s·g))	R_{31d}	R_{J33}	R_{E80}
Ta	3.1×10^9	1.00	1.45	—	2.6×10^8	1.00	1.05	—
W	2.2×10^9	1.00	1.06	1.00	6.2×10^8	1.00	0.60	1.00
Re	3.3×10^9	1.00	0.77	—	8.6×10^8	1.00	1.04	—
Pt	3.0×10^9	0.88	1.02	1.02	1.1×10^9	0.51	0.90	0.90
Au	1.2×10^9	1.00	—	—	2.2×10^9	1.00	—	—
Pb	2.6×10^9	1.00	—	0.97	3.6×10^8	1.00	—	1.07
Bi	4.8×10^9	1.00	—	0.96	8.5×10^8	1.00	—	0.24
Th	2.0×10^9	1.00	1.00	1.00	5.4×10^8	1.00	1.00	1.00
U	8.6×10^8	1.00	—	—	1.5×10^8	1.00	—	—

[a]In ENDF/B-VIII.0, ^{13}C (1.07% isotopic abundance) does not have proton production cross section and the alpha production cross section goes only up to 20 MeV.

Table 2. Same as table 1, but for deuterium, tritium, and ^{3}He.

Ele	^{2}H production Pr (at/(s·g))	R_{31d}	R_{J33}	R_{E80}	^{3}H production Pr (at/(s·g))	R_{31d}	R_{J33}	R_{E80}	^{3}He production Pr (at/(s·g))	R_{31d}	R_{J33}	R_{E80}
Li	4.2×10^{11}	1.00	—	—	1.7×10^{12}	1.00	—	—	1.1×10^9	1.00	—	—
Be	7.0×10^{10}	1.00	—	—	9.9×10^{10}	1.00	—	—	2.0×10^9	1.00	—	—
B	1.4×10^{11}	0.94	—	—	1.4×10^{11}	1.10	—	—	4.7×10^9	0.07	—	—
C	3.9×10^{10}	1.00	1.27	1.25[a]	4.1×10^9	1.00	—	—	4.5×10^8	1.00	—	—
N	1.2×10^{11}	1.00	0.74	0.74	3.9×10^{10}	1.00	1.04	1.04	7.0×10^8	1.00	—	—
O	5.0×10^{10}	0.97	0.97	0.97	4.0×10^9	1.44	1.44	1.43	1.2×10^9	—	—	—
F	5.4×10^{10}	1.00	—	—	2.2×10^{10}	1.00	—	—	—	—	—	—
Ne	2.7×10^{10}	—	1.00	1.00	5.5×10^9	—	1.00	1.00	1.3×10^9	—	1.00	1.00
Na	2.2×10^{10}	1.00	—	—	3.0×10^9	1.00	—	—	—	—	—	—
Mg	8.7×10^9	1.00	—	—	7.9×10^8	1.00	—	—	2.7×10^8	1.00	—	—
Al	3.6×10^{10}	1.00	1.00	1.00	3.9×10^9	1.00	1.00	1.00	—	—	—	—
Si	1.9×10^{10}	1.00	—	1.00	5.3×10^8	1.00	—	1.00	—	—	—	—
P	4.3×10^{10}	1.00	1.00	0.39	6.0×10^9	1.00	1.00	—	1.9×10^9	1.00	0.99	—
S	3.1×10^{10}	0.94	0.97	—	3.2×10^9	0.59	1.03	—	2.7×10^9	0.16	1.02	—
Cl	3.0×10^{10}	1.00	—	—	1.9×10^9	1.00	—	—	—	—	—	—
Ar	9.7×10^9	1.00	—	—	7.0×10^8	1.00	—	—	2.1×10^4	1.00	—	—
K	2.8×10^{10}	1.00	1.00	—	3.3×10^9	1.00	1.00	—	2.8×10^9	1.00	1.00	—
Ca	1.4×10^{10}	1.00	1.85	1.72	5.1×10^8	1.00	6.98	1.52	—	—	3.2×10^{9b}	4.4×10^{8b}
Sc	2.3×10^{10}	1.00	0.75	—	1.8×10^9	1.00	1.33	—	7.4×10^7	1.00	9.90	—
Ti	6.5×10^9	1.00	1.72	—	3.1×10^8	1.00	3.20	—	2.2×10^6	1.00	168.15	—
V	8.8×10^9	1.00	0.74	—	5.1×10^8	1.00	1.91	—	1.4×10^6	0.25	271.71	—
Cr	1.5×10^{10}	0.54	0.54	0.36	2.2×10^9	0.24	0.24	0.13	5.1×10^8	0.14	0.14	—
Mn	2.5×10^9	1.00	0.95	1.00	5.6×10^8	1.00	0.92	1.00	2.6×10^7	1.00	0.95	1.00
Fe	7.8×10^9	0.82	0.81	1.00	3.1×10^9	0.29	0.23	1.01	4.6×10^8	—	0.15	1.00
Co	6.5×10^9	1.00	—	—	6.7×10^8	1.00	—	—	1.1×10^5	1.00	—	—
Ni	1.1×10^{10}	1.00	—	0.89	3.5×10^8	1.00	—	1.13	—	—	—	—
Cu	8.5×10^9	1.00	2.47	0.92	4.9×10^8	1.00	3.12	1.57	1.1×10^6	1.00	69.93	—
Zn	6.8×10^9	1.00	1.20	—	3.8×10^8	1.00	3.04	—	1.7×10^6	1.00	423.81	—
Ga	5.8×10^9	1.00	1.07	—	6.8×10^8	1.00	2.45	—	5.6×10^5	1.00	704.03	—
Ge	3.8×10^9	1.00	1.04	—	8.5×10^8	1.00	0.88	—	4.1×10^7	1.00	4.78	—
Br	5.4×10^9	0.95	0.99	—	8.3×10^8	0.84	1.29	—	1.4×10^8	0.19	1.38	—
Y	4.2×10^9	0.57	—	—	1.4×10^9	0.29	—	—	1.4×10^8	0.15	—	—
Zr	3.5×10^9	1.00	1.59	—	4.7×10^8	1.00	1.60	—	1.2×10^8	1.00	0.14	—
Nb	5.3×10^9	1.00	0.97	0.74	6.9×10^8	1.00	0.74	0.60	1.6×10^8	1.00	3.27	—
Mo	2.9×10^9	1.00	—	—	2.3×10^8	1.00	—	—	3.6×10^5	1.00	—	—
Rh	6.3×10^9	1.00	—	—	1.2×10^9	1.00	—	—	2.0×10^7	1.00	—	—
Ag	1.8×10^9	1.00	—	—	5.8×10^8	1.00	—	—	1.7×10^7	1.00	—	—

Table 2. Continued.

| Ele | ^{2}H production | | | | ^{3}H production | | | | ^{3}He production | | | |
	Pr (at/(s·g))	R_{31d}	R_{J33}	R_{E80}	Pr (at/(s·g))	R_{31d}	R_{J33}	R_{E80}	Pr (at/(s·g))	R_{31d}	R_{J33}	R_{E80}
Cd	1.7×10^9	0.91	—	—	4.3×10^8	0.90	—	—	5.7×10^7	0.15	—	—
Sn	1.3×10^9	0.86	—	—	3.0×10^8	0.90	—	—	3.8×10^7	0.14	—	—
Sb	2.1×10^9	0.92	—	—	9.6×10^8	0.81	—	—	4.1×10^7	0.17	—	—
I	3.8×10^8	1.00	—	—	1.8×10^8	1.00	—	—	1.8×10^7	1.00	—	—
Cs	1.4×10^9	0.89	—	—	4.3×10^8	0.95	—	—	3.2×10^7	0.60	—	—
Ba	1.5×10^9	0.99	—	—	6.0×10^8	1.01	—	—	2.1×10^7	0.19	—	—
La	1.2×10^9	1.00	—	—	3.4×10^8	1.00	—	—	2.9×10^7	1.00	—	—
Ce	1.6×10^9	0.83	—	—	3.9×10^8	0.82	—	—	5.1×10^7	0.10	—	—
Sm	1.2×10^9	—	—	—	4.3×10^8	—	—	—	3.8×10^7	—	—	—
Gd	8.5×10^8	0.91	—	—	3.0×10^8	0.92	—	—	1.7×10^7	0.16	—	—
Er	7.5×10^8	0.89	—	—	2.7×10^8	0.90	—	—	1.5×10^7	0.15	—	—
Lu	1.0×10^9	0.89	1.06	—	4.5×10^8	0.83	1.08	—	2.1×10^7	0.16	1.00	—
Hf	8.6×10^8	0.91	—	—	3.4×10^8	0.89	—	—	1.5×10^7	0.16	—	—
Ta	4.2×10^8	1.00	2.14	—	8.5×10^7	1.00	2.15	—	1.2×10^6	1.00	1.30	—
W	—	—	$7.3 \times 10^{8\,b}$	—	—	—	$1.6 \times 10^{8\,b}$	—	—	—	$2.8 \times 10^{9\,b}$	—
Re	6.9×10^8	1.00	1.24	—	2.9×10^8	1.00	1.50	—	3.6×10^6	1.00	4.80	—
Pt	5.2×10^8	0.93	1.02	1.02	2.2×10^8	0.87	1.02	1.02	9.3×10^6	0.16	1.00	1.00
Au	1.3×10^8	1.00	—	—	2.3×10^7	1.00	—	—	6.4×10^5	1.00	—	—
Pb	8.1×10^8	1.00	—	0.89	3.2×10^8	1.00	—	0.61	1.9×10^6	1.00	—	—
Bi	2.1×10^9	1.00	—	0.38	8.7×10^8	1.00	—	0.12	4.1×10^6	1.00	—	0.00
Th	—	—	—	—	—	—	—	—	—	—	—	—
U	1.8×10^8	1.00	—	—	6.7×10^7	1.00	—	—	5.1×10^6	1.00	—	—

[a]The deuteron production in ^{13}C (1.07% isotopic abundance) is missing in ENDF/B-VIII.0.

[b]Absolute gas production values are provided, in atoms/(s·g), since these values are missing in FENDL-3.2.

the case of ENDF/B-VIII.0 and JEFF-3.3, all the most relevant isotopes that are part of the Eurofer-97 material have data up to at least 60 MeV.

Figure 13 shows how the cross sections in FENDL-3.1d, and to a lesser extent also those of JEFF-3.3, show discontinuities at 20 MeV. This is because, for some isotopes, the library has been built by putting together two different libraries: one below 20 MeV and others at higher energies. For example, ^{56}Fe in FENDL-3.1d is JEFF-3.1.1 up to 20 MeV and TENDL-2011 above. These discontinuities are no longer present in FENDL-3.2. This is because the nuclear data of some of the most relevant isotopes of the Eurofer-97 material (Fe and Cr) have been updated, adopting the results of the IAEA International Nuclear Data Evaluation Network (INDEN) [41], which is currently working on improving the evaluations of some materials (B, O, Si, Cr, Mn, Fe, Cu …). This work is a continuation of the one performed within the scope of the CIELO Project [42], which has recently made an important effort to improve the evaluations for Fe [43], among other materials, and whose results were adopted by ENDF/B-VIII.0.

Concerning the uncertainties in the gas production cross sections, we focused on the contribution of ^{56}Fe, as it is the most abundant isotope in Eurofer-97. FENDL-3.1d and FENDL-3.2 do not provide any uncertainty; ENDF/B-VIII.0 provides an uncertainty of $\sim$10% for both the H and He production cross sections in the energy range of interest; and these uncertainties in JEFF-3.3 are in the range of 5%–20%.

Finally, we extended the comparison to other materials. Tables 1 and 2 provide the gas production rates in all the elements available in FENDL-3.2 when placed in the central rigs of the HFTM. The values have been computed by multiplying the energy dependent neutron flux obtained from MCNP6.2 simulations, averaged inside the specimen rigs on the center, by the gas production cross sections (MT = 203–207 [31]) of the different neutron data libraries, and by an appropriate normalization factor in order to obtain the gas production in atoms per second and per material gram. The neutron flux corresponds to the one obtained with the FZK-2005 library to model the Li(d, xn) reactions and FENDL-3.1d for the neutron transport, i.e. the one labeled FZK-2005 on the left panel of figure 9 or as FENDL-3.1d on the left panel of figure 10. Natural isotopic abundances have been assumed, taken from the NIST database [44], which have been compiled from [45].

Missing values in the tables, shown with a em dash (—), correspond to missing information in the databases. In some cases there are no cross section for the production of a given particle, and in other cases the production cross section is provided only up to an incident energy not sufficient for fusion applications (typically 20 MeV). Specifically, we have established the arbitrary condition that, for each element, the cross sections of all the isotopes with isotopic abundances larger than 1% have to be defined at least up to 50 MeV. If this condition is not fulfilled then the corresponding gas production value does not appear in the tables. We made an exception with carbon, which has 1.07% of ^{13}C.

Tables 1 and 2 allow to calculate the gas production in many materials, identify which elements are the most relevant, and see the differences between the different libraries. For the case of Eurofer-97, it has been modeled with the following chemical composition in wt%: Fe (88.6%), Cr (9.0%), W (1.1%), Mn (0.4%), V (0.2%), Ta (0.12%), C (0.11%), Cu (0.10%), and other elements contributing no more than 0.05% each, and all together by less than 0.4%. From the values of the table (FENDL-3.2) it can be obtained that the main contributors to the He production are Fe (64%), C (21%), and Cr (11%), and that the ratios between the He production in ENDF/B-VIII.0 and JEFF-3.3, for these isotopes, are 1.14 (Fe), 1.39 (C), and 0.98 (Cr). Thus, the 10%–12% larger He production in ENDF/B-VIII.0 with respect to JEFF-3.3 is mainly due to differences in the He production cross sections of Fe and C.

5. Summary and conclusions

In this work we investigated how the differences between nuclear data evaluations are propagated to the results of IFMIF-DONES neutronic calculations.

First, we studied how well different nuclear models and evaluations are able to reproduce experimental results of the neutron production due to 40 MeV deuterons impinging on a thick lithium target. The conclusion is that the two publicly available deuteron incident evaluations, FZK-2005 and JENDL/DEU-2020, reproduce the experimental data much better than the models available to date in Geant4 and MCNP6.2. We estimated in ∼15% the uncertainty, which is obtained when using these evaluations to compute the number of neutrons in the megaelectronvolt range emitted between 0° and 20° with respect to the deuteron beam, which are the most relevant for material analysis at IFMIF-DONES. This uncertainty is dominated by the uncertainty of the experimental data available. Consequently, to reduce this uncertainty, new Li(*d, xn*) measurements are needed.

This part of the work has also served to validate the performance of Geant4 and MCNP6.2 when using deuteron incident data libraries. In order to obtain satisfactory results it has been necessary to correct part of the NJOY and Geant4 codes. The rest of the work has been made with MCNP6.2, but this validation may be useful for future works using Geant4. Indeed, JENDL/DEU-2020 has been included in the data library distributed together with Geant4.11.0 (December 2021 release).

In the second part of the study, we performed MCNP6.2 simulations of the full IFMIF-DONES geometry. The same simulation has been carried out with different deuteron data libraries to model the Li(*d, xn*) reactions (FZK-2005, JENDL/DEU-2020 and a third neutron source, 2D-Hagiwara, built from the experimental data reported by Hagiwara *et al*), and with different neutron data libraries for the neutron transport (FENDL-3.1d, ENDF/B-VIII.0, JEFF-3.3 and JENDL-4.0). We then compared the neutron flux, primary displacement damage, gas production, and nuclear heating in the HFTM obtained with the different libraries.

One of the first conclusions we obtained is that the calculated neutron flux inside the HFTM depends much more on the deuteron data library (i.e. on the neutron source) than on the neutron transport library. The reason is that the dimensions of the HFTM are comparable with the mean free paths of the generated neutrons. Another result is that, when we compare the results of simulations performed with different deuteron libraries (using the same neutron library), then the obtained differences do not depend significantly on the neutron library used. The same thing happens the other way around. When results obtained with different neutron libraries (using the same deuteron library) are compared, the differences, again, do not depend significantly on the deuteron library used.

Regarding the differences obtained when using different deuteron libraries, the results (neutron flux, primary displacement damage, gas production, and nuclear heating) are compatible within ∼10% in the central part of the HFTM, i.e. in the irradiation zone, and they differ by up to 60% on the sides, intended for diagnosis or lateral neutron reflectors. The results obtained with the 2D-Hagiwara neutron source are much closer to the ones from JENDL/DEU-2020 than those of FZK-2005, and we attribute this to the fact that the neutron production in FZK-2005 is larger at small neutron energies and at large angles than the one reported by Hagiwara *et al*. This indicates that probably the best results are obtained with JENDL/DEU-2020, and we estimate the uncertainty in the resulting neutron flux inside the HFTM in ∼15%.

Regarding the neutron transport libraries, we found that the differences in the neutron flux inside the HFTM when using one or another library are very small, of the order of 1%. However, some quantities, such as the H and He production differ significantly, by up to ∼10% in Eurofer-97. This occurs due to differences in the gas production cross sections of the different neutron libraries. These differences are compatible within the uncertainties reported by the evaluated libraries, which are of the order of 10%–20%. In order to quantify these differences in different materials, we generated data tables with the gas production rates in many chemical elements, computed with different data libraries and with the neutron flux obtained in the specimen rigs on the central part of the HFTM.

In this case it is not straightforward, at least for us, to decide which neutron transport library provides the most reliable results. What we have seen is that FENDL-3.2 seems to have improved the data compared to FENDL-3.1d, and also that JENDL-4.0 is not an appropriate library to perform these calculations, since the data only goes up to 20 MeV. We would like to mention, however, that after this work was finished, a new version of JENDL was released, JENDL-5, with data up to 200 MeV [46, 47].

The results of this work, in addition to quantifying the differences in neutronic calculations due to the libraries used, provide, to a certain extent, an estimate of the confidence margins of these neutronic calculations. These margins are acceptable from the point of view of the design of the IFMIF-DONES HFTM, and can be used to optimize the placement of

the samples inside the rigs, as well as to better determine the irradiation times.

Acknowledgments

ORCID iDs

E. Mendoza https://orcid.org/0000-0002-2843-1801
D. Cano-Ott https://orcid.org/0000-0002-9568-7508
A. Ibarra https://orcid.org/0000-0002-2420-2497
F. Mota https://orcid.org/0000-0002-1337-2482
I. Podadera https://orcid.org/0000-0002-3459-4631

References

[1] Ibarra A. *et al* 2018 *Nucl. Fusion* **58** 105002
[2] Federici G. *et al* 2018 *Fusion Eng. Des.* **136** 729–41
[3] Werner C.J. *et al* 2018 *MCNP Version 6.2 Release Notes (LA-UR-18-20808)* (Los Alamos National Laboratory) (https://laws.lanl.gov/vhosts/mcnp.lanl.gov/pdf_files/la-ur-18-20808.pdf)
[4] Sauvan P., Sanz J. and Ogando F. 2010 *Nucl. Instrum. Methods Phys. Res.* A **614** 323–30
[5] Simakov S.P., Fischer U., Kondo K. and Pereslavtsev P. 2012 *Fusion Sci. Technol.* **62** 233–9
[6] Pereslavtsev P., Fischer U., Simakov S. and Avrigeanu M. 2008 *Nucl. Instrum. Methods Phys. Res.* B **266** 3501–12
[7] Fischer U., Avrigeanu M., Pereslavtsev P., Simakov S.P. and Schmuck I. 2007 *J. Nucl. Mater.* **367–370** 1531–6
[8] Forrest R., Capote R., Otsuka N., Kawano T., Koning A., Kunieda S., Sublet J.C. and Watanabe Y. 2012 *FENDL-3 Library Summary Documentation Tech. Rep. 6410 INDC(NDS)-0628* (Vienna: IAEA)
[9] *The Fusion Evaluated Nuclear Data Library,FENDL-3.1d* (https://nds.iaea.org/fendl31d/)
[10] Otuka N. *et al* 2014 *Nucl. Data Sheets* **120** 272–6
[11] Hagiwara M., Itoga T., Kawata N., Hirabayashi N., Oishi T., Yamauchi T., Baba M., Sugimoto M. and Muroga T. 2005 *Fusion Sci. Technol.* **48** 1320–8
[12] Hagiwara M. *et al* File EXFOR E1986.002 retrieved from the IAEA Nuclear Data Services website (http://nds.iaea.org/EXFOR/E1986.002)
[13] Saltmarsh M.J., Ludemann C.A., Fulmer C.B. and Styles R.C. 1977 *Nucl. Instrum. Methods* **145** 81–90
[14] Fischer U., Simakov S.P., Konobeyev A., Pereslavtsev P. and Wilson P. 2002 *Fusion Eng. Des.* **63–64** 493–500
[15] Mann F., Schmittroth F. and Carter L. 1981 Neutrons from d + Li and the FMIT irradiation environment *Tech. Rep. 6410 HEDL-TC-1459* Hanford Engineering Development Laboratory (Richland, Washington)

[16] Mota F., Ibarra Á., García Á. and Molla J. 2015 *Nucl. Fusion* **55** 123024
[17] Mota F. and Molla J. 2016 *Fusion Eng. Des.* **109–111** 1212–6
[18] Qiu Y., Arbeiter F., Fischer U. and Schwab F. 2018 *Nucl. Mater. Energy* **15** 185–9
[19] Fischer U., Bienkowska B., Drozdowicz K., Frisoni M., Mota F., Ogando F., Qiu Y., Stankunas G. and Tracz G. 2019 *Fusion Eng. Des.* **146** 1276–81
[20] Frisoni M., Bernardi D. and Nitti F.S. 2020 *Fusion Eng. Des.* **157** 111658
[21] Nakayama S., Iwamoto O., Watanabe Y. and Ogata K. 2021 *J. Nucl. Sci. Technol.* **58** 805–21
[22] Nishitani T., Yoshihashi S., Kumagai K., Kondo K. and Uritani A. 2021 *Plasma Fusion Res.* **16** 1405104
[23] Chadwick M. *et al* 2011 *Nucl. Data Sheets* **112** 2887–996
[24] Koning A.J., Rochman D., Sublet J.-C., Dzysiuk N., Fleming M. and van der Marck S. 2019 *Nucl. Data Sheets* **155** 1–55
[25] Koning A.J., Hilaire S. and Duijvestijn M.C. 2007 *TALYS-1.0 Proc. Int. Conf. Nuclear Data for Science and Technology* (Nice, France April 2007) pp 211–4
[26] Rochman D. and Koning A.J. 2012 TENDL-2011: TALYS-based evaluated nuclear data library *PHYSOR 2012: Conf. Advances in Reactor Physics - Linking Research, Industry, and Education* (Knoxville, TN (United States)) April 2012)
[27] Koning A. and Rochman D. 2020 private communication
[28] *The Fusion Evaluated Nuclear Data Library* FENDL-3.2 (https://nds.iaea.org/fendl/)
[29] Agostinelli S. *et al* 2003 *Nucl. Instrum. Methods* A **506** 250–303
[30] Allison J. *et al* 2016 *Nucl. Instrum. Methods* A **835** 186–225
[31] Trkov A. *et al* 2018 *ENDF-6 Formats Manual Tech. Rep. BNL-203218-2018-INRE* Brookhaven National Laboratory (https://nndc.bnl.gov/csewg/docs/endf-manual.pdf)
[32] 2020 *JENDL Deuteron Reaction Data File* (https://ndc.jaea.go.jp/ftpnd/jendl/jendl-deu-2020.html)
[33] Macfarlane R., Muir D.W., Boicourt R.M., Kahler III A.C. and Conlin J.L. 2017 *The NJOY Nuclear Data Processing System, Version 2016 Tech. Rep. LA-UR-17-20093* Los Alamos National Laboratory (US) (https://doi.org/10.2172/1338791)
[34] Mendoza E., Cano-Ott D., Koi T. and Guerrero C. 2014 *IEEE Trans. Nucl. Sci.* **61** 2357–64
[35] Hashimoto S., Iwamoto Y., Sato T., Niita K., Boudard A., Cugnon J., David J.-C., Leray S. and Mancusi D. 2014 *Nucl. Instrum. Methods Phys. Res.* B **333** 27–41
[36] Plompen A. *et al* 2020 *Eur. Phys. J.* A **56** 181
[37] *JEFF-3.3, NEA Data Bank, dpa Data Sub-Library* (https://oecd-nea.org/dbdata/jeff/jeff33/#dpa)
[38] Mergia K. and Boukos N. 2008 *J. Nucl. Mater.* **373** 1–8
[39] Brown D. *et al* 2018 *Nucl. Data Sheets* **148** 1–142
[40] Shibata K. *et al* 2011 *J. Nucl. Sci. Technol.* **48** 1
[41] Capote R., Dimitriou P. and Schnabel G. *INDEN - International Nuclear Data Evaluation Network* (https://nds.iaea.org/INDEN/)
[42] Chadwick M. *et al* 2018 *Nucl. Data Sheets* **148** 189–213
[43] Herman M. *et al* 2018 *Nucl. Data Sheets* **148** 214–53
[44] Coursey J.S., Schwab D.J., Tsai J.J. and Dragoset R.A. Atomic weights and isotopic compositions with relative atomic masses (https://nist.gov/pml/atomic-weights-and-isotopic-compositions-relative-atomic-masses)
[45] Berglund M. and Wieser M.E. 2011 *Pure Appl. Chem.* **83** 397–410
[46] Iwamoto O., Iwamoto N., Shibata K., Ichihara A., Kunieda S., Minato F. and Nakayama S. 2020 *EPJ Web Conf.* **239** 09002
[47] *JENDL5* (https://ndc.jaea.go.jp/jendl/j5/j5.html)